ACS OMEGA

http://pubs.acs.org/journal/acsodf

Article

Defect-Induced Adsorption Switching (p- to n- Type) in Conducting Bare Carbon Nanotube Film for the Development of Highly Sensitive and Flexible Chemiresistive-Based Methanol and NO_2 Sensor

Jyoti Prakash,* Pandugula Thirmaleshwar Rao, Rohan Rohilla, Divya Nechiyil, Manmeet Kaur, Kailasa S. Ganapathi, Anil Krishna Debnath, Amit Kaushal, Jitendra Bahadur, and Kinshuk Dasgupta

Cite This: *ACS Omega* 2023, 8, 6708−6719

Read Online

ACCESS | Metrics & More | Article Recommendations | Supporting Information

ABSTRACT: Lightweight and flexible gas sensors are essentially required for the fast detection of toxic gases to pass on the early warning to deter accident situations caused by gas leakage. In view of this, we have fabricated a thin paper-like free-standing, flexible, and sensitive carbon nanotube (CNT) aerogel gas sensor. The CNT aerogel film synthesized by the floating catalyst chemical vapor deposition method consists of a tiny network of long CNTs and ∼20% amorphous carbon. The pores and defect density of the CNT aerogel film were tuned by heating at 700 °C to obtain a sensor film, which showed excellent sensitivity for toxic NO_2 and methanol gas in the concentration range of 1−100 ppm with a remarkable limit of detection ∼90 ppb. This sensor has consistently responded to toxic gas even after bending and crumpling the film. Moreover, the film heat-treated at 900 °C showed a lower response with opposite sensing characteristics due to switching of the semiconductor nature of the CNT aerogel film to n-type from p-type. The annealing temperature-based adsorption switching can be related to a type of carbon defect in the CNT aerogel film. Therefore, the developed free-standing, highly sensitive, and flexible CNT aerogel sensor paves the way for a reliable, robust, and switchable toxic gas sensor.

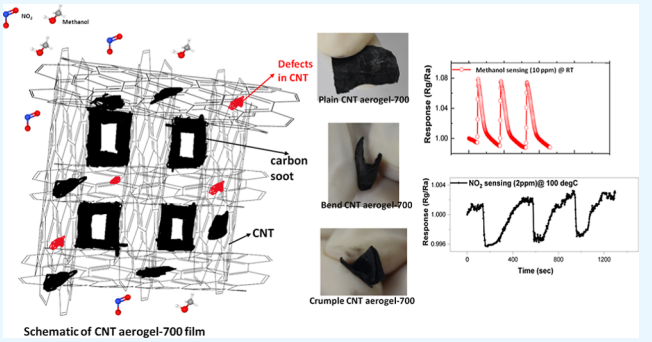

1. INTRODUCTION

The robust, flexible, portable, and wearable gas sensors are gaining importance for real-time and on-site detection of hazardous gases to provide a rapid alert on the environmental quality.[1,2] The compatible and easy-to-use transducer in a flexible and wearable sensor is mostly a chemiresistor-based semiconductor.[3] Therefore, different types of chemiresistance-based metal oxide[4,5] and polymer composite[6,7] gas sensors are being studied. The metal oxide semiconductor-based sensors are most widely used but lack flexibility, primarily operate at elevated temperatures, and are sensitive to environmental factors. On the other hand, flexible polymer composite-based devices can be used as wearable devices but lack sensitivity and durability. Due to the need for detection besides gas concentration measurement at room temperature in low concentrations with quick response time, flexible sensors based on materials such as carbon nanotubes (CNT),[8] silicon carbide,[9] graphene oxide,[10] and porous polymer fibers[11] are being explored. Among these, CNTs are the most explored sensing material in the chemiresistor-based sensors because they can provide high sensitivity due to high aspect ratio, high selectivity with possible functionalization, and room-/low-temperature device operation. Zhang et al.[12] reported that the continuous thin CNT conducting film has a better response for ethanol sensing than scattered deposited CNT on the cellulose film. It has been highlighted that film thickness plays a crucial role and a thicker film might degrade the sensor response. Xue et al.[13] fabricated a flexible polyaniline/CNT nanocomposite film by the solution processing route for sensing ammonia gas. Agarwal et al.[14] fabricated a spray-coated single-walled CNT−polytetrafluoroethylene membrane as a flexible sensor for selective and sensitive detection of NO_2 gas at room temperature. McConnell et al.[15] fabricated the free-standing CNT−palladium composite sheet-based hydrogen sensor by electroplating palladium onto high-purity CNTs drawn from a dense, vertically aligned array grown by chemical vapor deposition on silicon substrates. Geng et al.[16] have fabricated

Received: November 15, 2022
Accepted: January 27, 2023
Published: February 9, 2023

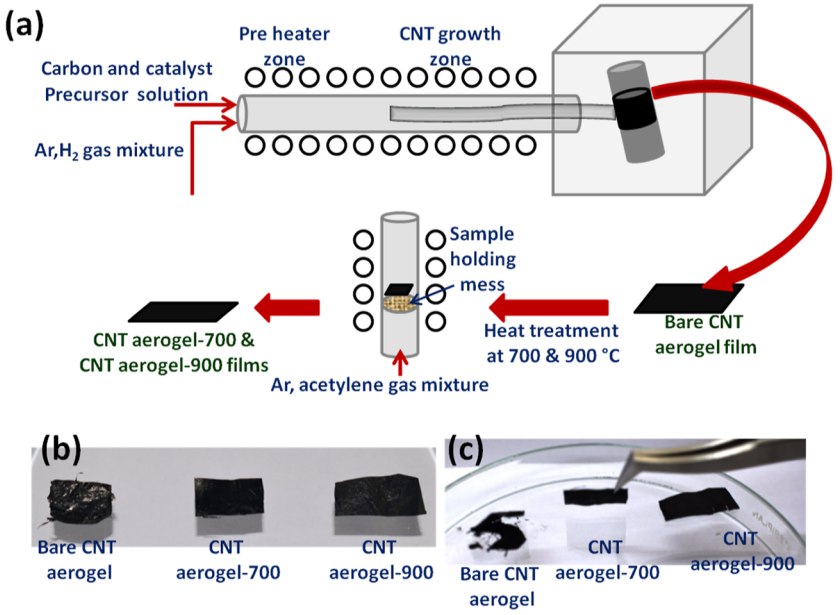

Figure 1. (a) Schematic of the fabrication process of bare and treated CNT aerogel films using the FCCVD process; pictures of (b) fabricated CNT aerogel films and (c) CNT aerogel films on glass slide after soaking in acetone.

flexible printed CNT−TFTs using the printing process to selectively deposit semiconducting CNTs in device channels and sensor showed extremely high sensitivity to H2S at room temperature. Chang et al.[17] reported a CNTs anatase titanium dioxide film-based flexible NO gas sensor using the CVD method to grow the CNT network and followed by in situ hydrolysis and calcination. Recently, Seo et al.[18] reported a one-pot hydrothermal synthesis process for the fabrication of indium oxide/single-walled CNT heterostructure FET NO_2 gas sensors. The flexibility was introduced into the sensor by making In_2O_3/SWNT composite with an epoxy gate dielectric and demonstrated superior response and recovery performance when compared to conventional SWNT FET gas sensors.

As discussed above, the present CNT-based gas sensing utilizes mostly a printed circuit platform, polymer composite, and carbon fiber cloth as a substrate to obtain a flexible sensor device. In such sensors, the electrical conductance change caused by the gas adsorption is measured to detect the gases. This means that the sensor response can be dependent on the number of CNTs, its alignment, inter-CNT junctions, and bridging of CNT over the metal electrodes connected to the external measuring instruments. This leads to degrading the sensor performance for repeated and long-term sensing of gases. Moreover, the effects of the above factors have not been channelized to obtain an economical ultra-sensitive sensor, which might be due to the difficulty in processing CNT to obtain its uniform, defined, and flexible freestanding electrical conducting network. There has been no effective way to control and quantify the number of CNTs retained on the sensor electrode.

To address drawbacks of present CNT-based sensors, a promising technology capable of fulfilling these requirements has been realized by synthesizing a miniaturized, economical, and flexible CNT aerogel film. The floating catalyst chemical vapor deposition process was used to control and alter the morphology and orientation of CNTs to fine-tune the gas sensing properties. The developed CNT aerogel sensor has been used for sensing methanol and nitrogen dioxide (NO_2) in a different configuration like bend and crumpled samples. In the advancement of the gas sensors field, recently p- to n-type transition characteristics of the metal oxide semiconductor-based gas sensors have been reported.[19] There are only a few reports on this and most of them are related to the p- to n-transition specifically due to exposure to a particular gas/vapor at a transition temperature and the complex galvanic replacement reaction involving a p-type and n-type sensor material. In our work, p- to n-type transition behavior and its sensing mechanism have been correlated to the defect-induced switching on the CNT during the gas adsorption process. To the best of our knowledge, we are demonstrating for the first time the switching of the gas adsorption process followed by p- to n-type transition, controlled by defects present on the CNT film. The defect-induced adsorption switching mechanism plays a leading role in determining the response of the sensor for the room as well as low-temperature applications. Thus, our synthesized prototype standalone and flexible bare CNT film-based sensor suitable for wearable sensing device applications and defects-driven adsorption switching will be of greater interest to the scientific community.

2. EXPERIMENTAL SECTION

2.1. Synthesis of the Bare and Treated CNT Aerogel Film. The flexible and free-standing CNT aerogel film was synthesized using optimized synthesis parameters as reported by us elsewhere[20] using a floating catalyst chemical vapor deposition process (Figure 1a). In short, the carbon source precursor ethyl alcohol mixed with catalyst precursor ferrocene and promoter precursor thiophene to obtain C/Fe/S = 32:2:0.3 wt % ratio in the solution. The precursor solution was passed at a rate of 1 mL/h through a pre-heater (150 °C) to the CNT growth zone (1250 °C; 100 cm) using an argon and hydrogen mixture (1:1) as the carrier gas with a 1 lpm flow rate. The synthesized CNT aerogel film was collected on a rotating drum and later on carved into several pieces of size: 1 × 1.2 cm^2 to use as the sensor. These CNT aerogel films were termed bare CNT aerogel films. Further bare CNT aerogel

https://doi.org/10.1021/acsomega.2c07314
ACS Omega 2023, 8, 6708−6719

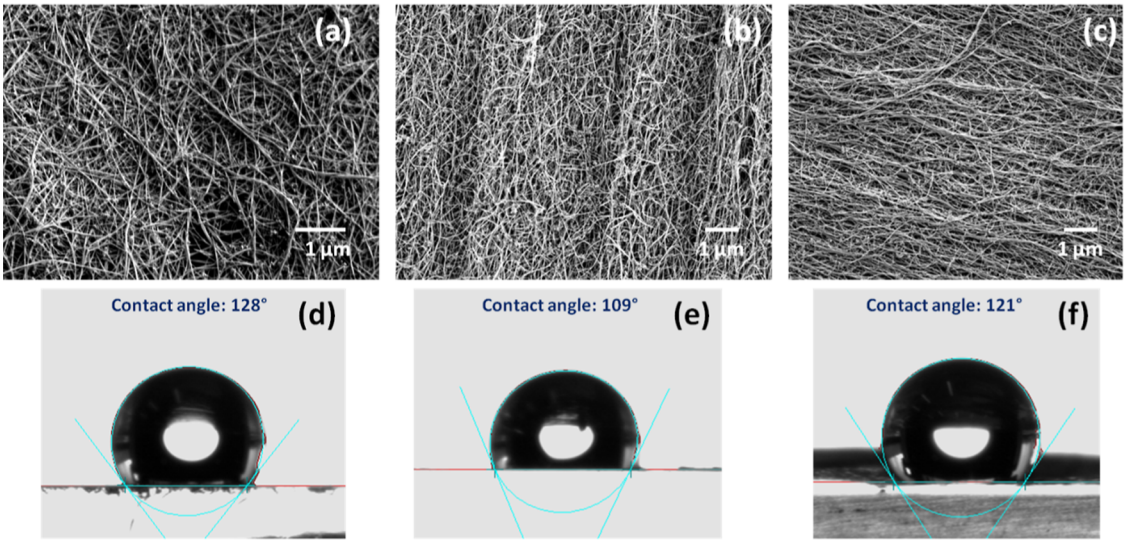

Figure 2. SEM image and contact angle of the surface of (a,d) bare, (b,e) CNT aerogel-700, and (c,f) CNT aerogel-900 films, respectively.

films were heat treated at 700 and 900 °C for 15 min in flowing argon (2 lpm) and acetylene (50 sccm) mixed gas. Throughout the paper, the bare CNT aerogel film treated at 700 and 900 °C is termed as CNT aerogel-700 and CNT aerogel-900, respectively. The electrical conductivity of the CNT aerogel film in a two-electrode configuration was studied (for details, see Supporting Information, Figure S1).

2.2. Sample Characterization. The surface of bare and treated CNT aerogel films were analyzed under a scanning electron microscope at an accelerated voltage of 10 kV (JSM-7600F-JEOL Inc.). The defects and porosity in the CNT aerogel film were analyzed using confocal Raman microscopy (WITec alpha-300R, GmbH equipped with a 532 nm laser) and SAXS instrument (CuKα micro-focus source).

2.3. Sensing Performance Analysis. The methanol gas sensing measurements were performed in a dynamic environment. The schematic of the dynamic environment sensing system and its operation is provided in Supporting Information, Figure S2. In brief, the sensing measurements were carried out at one particular concentration (10 ppm) in repeated cycles by turning gas ON and OFF in the sensing chamber at room temperature (28 °C) and relative humidity (RH) of 45%. Every measurement was replicated at least three times in order to assess its reproducibility. Later on, the sensing performance of sensors was tested by increasing concentrations of the methanol in the sensor chamber (i.e., 1, 2.5, 5, 10, 20, 40, 80, and 100 ppm). Calibrated mass flow controllers (accuracy: ±1%) were used to ensure the reproducibility of such tests. The change in resistance of the active layers caused by the presence of the different gases was measured using an electrochemical workstation (CHI 760E, USA) in a two-electrode configuration (Supporting Information, Figure S2). The gas sensing behavior was further measured in different operating temperatures and humidity conditions.

The NO_2 gas sensing measurements were performed in a static environment method (Supporting Information, Figure S3) as reported elsewhere.[21] In brief, the sensor film is connected to the alumina sensing platform using copper wire and connecting it to the film using a silver paste. A Pt wire heater was attached at the backside of the alumina substrate to maintain and control the operating temperature of the sensor. The sensor films were mounted upside down in a leak-tight stainless steel chamber having a volume of 250 cm^3. The required concentration of a test gas in the chamber was attained by introducing a measured quantity of desired gas using a syringe. The response curves toward various test gases were measured by applying a fixed bias of 0.1 V across the electrode and the time dependence of the current was recorded using PC based data acquisition system using LabVIEW software. Once a steady state was achieved, recovery of sensors was recorded by exposing the sensors to air, which is achieved by opening the lid of the chamber.

The gas sensor response is plotted as R_g/R_a versus time, where R_g is the sensor resistance when exposed to the analyte gas and R_a is the sensor initial resistance in air, that is, before exposure to analyte gas. Response and recovery times were defined as the times needed for 90% of a total change in resistance upon exposure to test gas and fresh air, respectively.

3. RESULTS AND DISCUSSION

The bare CNT aerogel film was synthesized using floating catalyst chemical vapor deposition, as shown in Figure 1a. This method shows a simple process for the integration of individual CNT to form a freestanding and flexible CNT film without using polymer or other support. The bare CNT aerogel film was further treated at 700 and 900 °C in presence of an argon and acetylene gas mixture. The purpose of using an acetylene gas (2.5%) mixture is to slightly deposit carbon soot/amorphous carbon in the pores of the CNT network to enhance the gas adsorption performance of the CNT aerogel film. The synthesized bare CNT aerogel, CNT aerogel-700, and CNT aerogel-900 films are shown in Figure 1b. The bare CNT aerogel film normally sticks to the glass/silicon and another substrate if wetted with ethanol or acetone. Therefore, it poses difficulty in transferring CNT aerogel film from one substrate to another; moreover, this can hamper the long-term performance of the bare CNT aerogel film as a sensor. However, treated CNT aerogel films (CNT aerogel-700 and 900) do not stick to the glass or other substrate's surface, as shown in Figure 1c. The stickiness behavior of the bare and treated films are further shown in a video provided as Supporting Information. It was observed that the temperature treatment of the bare CNT aerogel film cures the film in such a

https://doi.org/10.1021/acsomega.2c07314
ACS Omega 2023, 8, 6708−6719

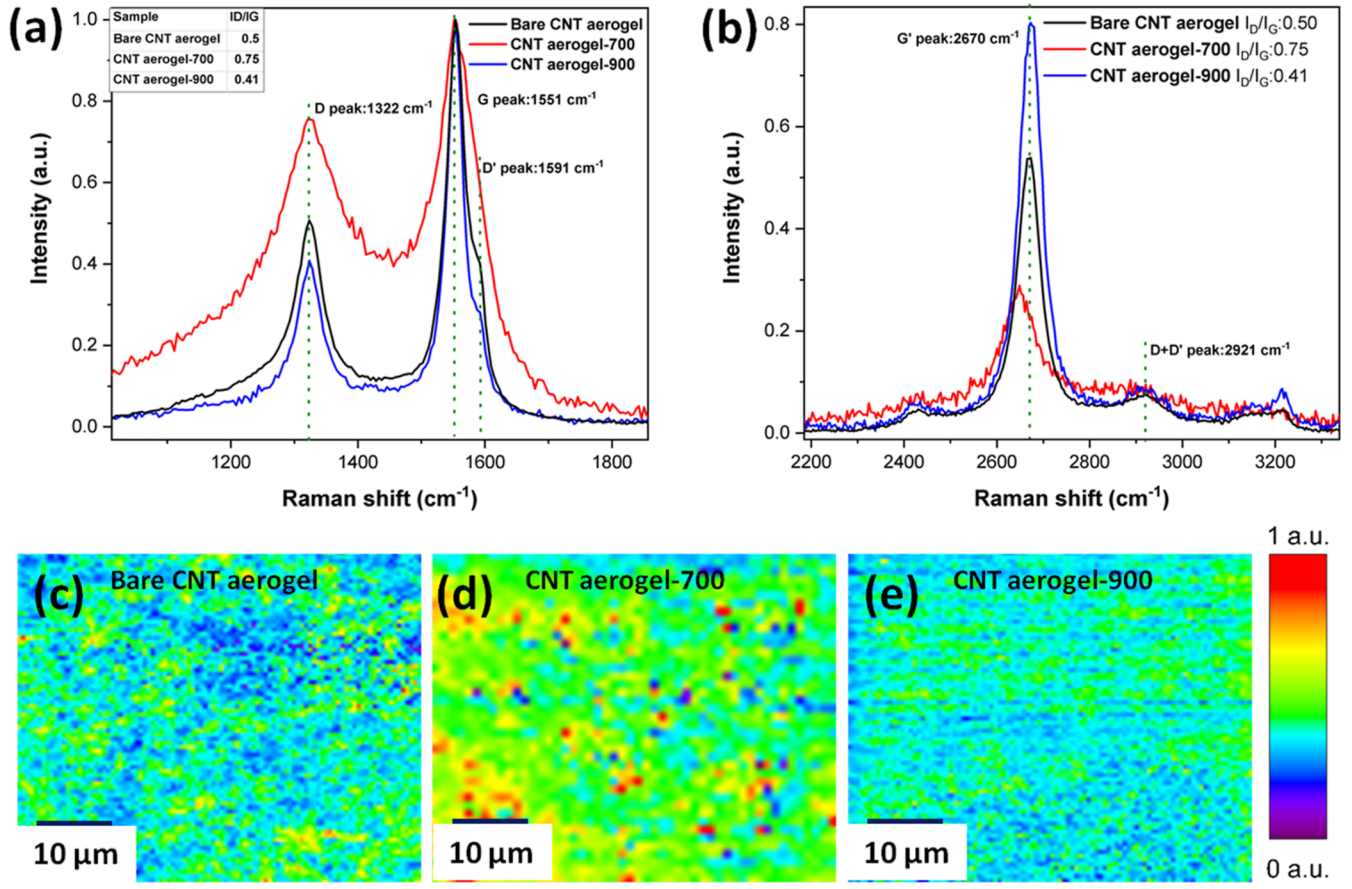

Figure 3. (a,b) Raman spectra and (c−e) Raman mapping of the bare and heat-treated CNT aerogel films.

way that it does not stick to the surfaces and is easy to transfer from one substrate to other.

The scanning electron microscopy (SEM) images of the bare CNT aerogel film in Figure 2a show that it comprises a condensed and arbitrarily distributed network of CNT. The maze of CNTs in the film provides its free-standing and flexible characteristics. There is no visible change in the arrangement of CNTs in the CNT aerogel film after heat treatment (Figure 2b,c). The surface morphology of CNT aerogel film does not change after heat treatment, which may be due to the excellent mechanical integrity of CNTs. However, the surface wetting characteristics change after heat treatment, as shown by the contact angle measurement in Figure 2. It has been observed that the bare CNT aerogel film surface is hydrophobic and turns toward the hydrophilic nature for the CNT aerogel-700 film. However, the surface of CNT aerogel-900 film turns back to the hydrophobic nature.

The defects in bare and treated CNT aerogel films were analyzed using Raman spectra as shown in Figure 3a,b. It is observed that the D, G, D′, and G′ peaks corresponding to CNT/amorphous carbon appear around ∼1322,∼1551, ∼1591, and 2670 cm^{-1}, respectively, for all CNT aerogel films. The presence of G and D/D′/D + D′ peaks in Raman spectra confirms the presence of sp^2 and sp^3 carbon networks, respectively. The integrated intensity ratio of D and G peaks showed that the heat treatment increases defect density in the CNT aerogel-700 film (Figure 3a). However, the D, D′ peak, and I_D/I_G intensity drastically decreases with 900 °C heat treatment. The G′ peak intensity increment for CNT aerogel-900 confirms the annealing of defects and formation of a more graphitic structure. However, CNT aerogel-700 showed a decrease in G′ peak intensity. This confirms that the heat-treated CNT aerogel-700 sample consists of amorphous carbon along with CNTs, whereas in the CNT aerogel-900 sample, defects on CNTs were annealed and consisted a low concentration of amorphous carbon. The distribution of defect over the surface of samples are further confirmed by Raman mapping of the bare and treated CNT aerogel samples, as shown in Figure 3d,e. It is observed that the defect density was highest for CNT aerogel-700 samples and uniformly distributed over the film surface.

The bulk porosity and specific surface area of bare and treated CNT aerogel films were further analyzed using SAXS (Figure 4a,b) and BET technique (Supporting Information, Figure S5). The specific surface area of CNT aerogel-700 samples (∼432 m^2/g) is much higher than that of the bare (∼257 m^2/g) and CNT aerogel-900 samples (∼301 m^2/g). The CNT aerogel-700 has shown remarkably highest surface area than other samples due to the generation of accessible sites for adsorption via defects/amorphous carbon and pore architecture. It was observed from SAXS studies that all three samples showed the bi-modal distribution of pores in the bulk of the films (Supporting Information). The estimated pore size distribution is plotted in Figure 4b. In the bare CNT aerogel film, the pore sizes are distributed in ∼7 nm and ∼30 nm regions. The CNT aerogel-700 sample showed a decrease in pore sizes, whereas the pore sizes in the CNT aerogel-900 sample increased. The change in porosity of heat-treated samples might be related to the annealing of defects and carbonization of aromatic carbon. The quantitative analysis of

https://doi.org/10.1021/acsomega.2c07314
ACS Omega 2023, 8, 6708−6719

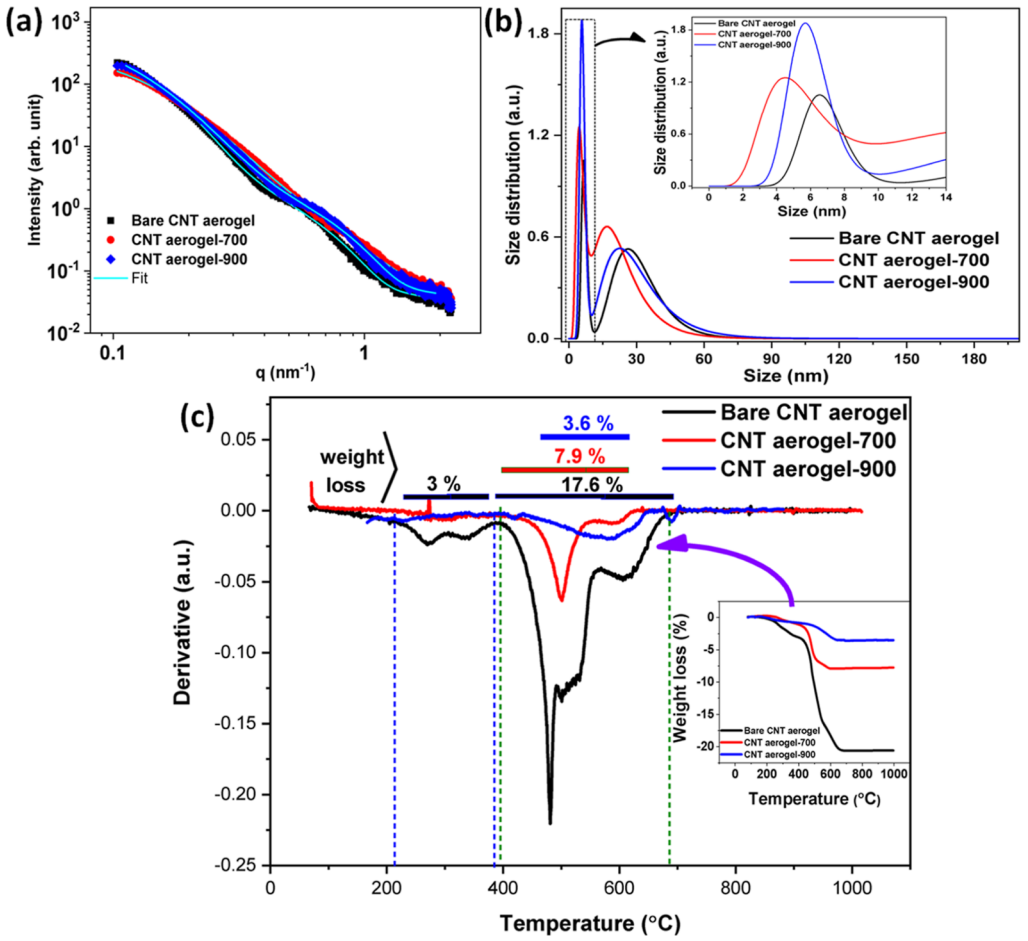

Figure 4. (a) SAXS analysis plot, (b) estimated pore size distribution plot, and (c) TG/DTA plot of the bare and heat-treated CNT aerogel films.

defects and amorphous/aromatic carbon present in bare and heat-treated CNT aerogel samples was carried out using the thermogravimetric method. Figure 4c shows the differential of thermogravimetric (DTG) curves of bare and treated CNT aerogel samples, and the inset shows the temperature versus weight loss. It is seen from the inset thermogravimetric curve that the bare CNT aerogel sample starts losing weight from ∼150 °C, and major weight loss occurred from 400 to 680 °C. The total weight loss observed in bare CNT aerogel samples is ∼20%. This result has confirmed that bare CNT aerogel samples synthesized by the FCCVD method using ethanol precursor contain ∼20% amorphous carbon. The formation of amorphous carbon during CNT synthesis has been explained based on the decomposition mechanism of ethanol. It has been reported in the literature that during the decomposition of ethanol at 1200 °C, the following three major steps are involved: (i) initial formation of lower-molecular-weight hydrocarbons (i.e., CH_4, C_2H_4, C_2H_6, C_6H_6, etc.) and (ii) later on their recombination to produce larger hydrocarbons and polycyclic aromatic hydrocarbon (PAH) and (iii) further pyrolysis of PAH forms carbon soot.[22,23] The weight losses of the bare CNT aerogel sample in different temperature zones (Figure 4) are analyzed as follows: (i) there is a 3% weight loss at low temperature ∼265/335 °C may be due to the release of adsorbed moisture and volatile organic components and (ii) the major weight loss observed between 400 and 680 °C might be due to carbonization of amorphous carbon (hydrocarbon and PAH) and curing of CNT defects present in the bare CNT aerogel sample. Therefore, bare CNT aerogel film consists of amorphous carbon (hydrocarbon/PAH/soot) along with a network of CNTs. The presence of a substantial amount of amorphous carbon specially PAH leads to the stickiness nature of the CNT aerogel film, as observed in Figure 1c.

The CNT aerogel-700 and CNT aerogel-900 samples showed 7.9 and 3.6% weight loss during thermogravimetric analysis (inset Figure 4c), respectively. As observed from the DTG curve, the CNT aerogel-900 sample losses weight at high temperatures in comparison to the CNT aerogel-700. In the case of the CNT aerogel-700 sample, the heating of the CNT aerogel sample at 700 °C in a diluted acetylene gas atmosphere leads to carbonization of hydrocarbons/PAHs to form carbon soot,[24] simultaneous cracking of acetylene can also form the soot,[25,26] and curing of CNT defects. In the case of the CNT aerogel-900 sample, the heating of the CNT aerogel sample at 900 °C in a diluted acetylene gas atmosphere lead to the carbonization of hydrocarbons/PAHs to carbon soot having a more ordered phase[24] and simultaneous decomposition of acetylene can lead to forming ordered phase pyrolytic carbon.[27,28] This might be the reason for a drastic reduction in defect density (Figure 3), low weight loss in the thermogravimetric experiment (Figure 4c), and change in surface wetting behavior (Figure 2f) of the CNT aerogel-900 sample. The decrease in pore size of the CNT aerogel-700 sample (SAXS data: Figure 3e) showed that heat treatment at 700 °C facilitate the formation of carbon soot in the network of CNTs by carbonization of amorphous carbon and

https://doi.org/10.1021/acsomega.2c07314
ACS Omega 2023, 8, 6708−6719

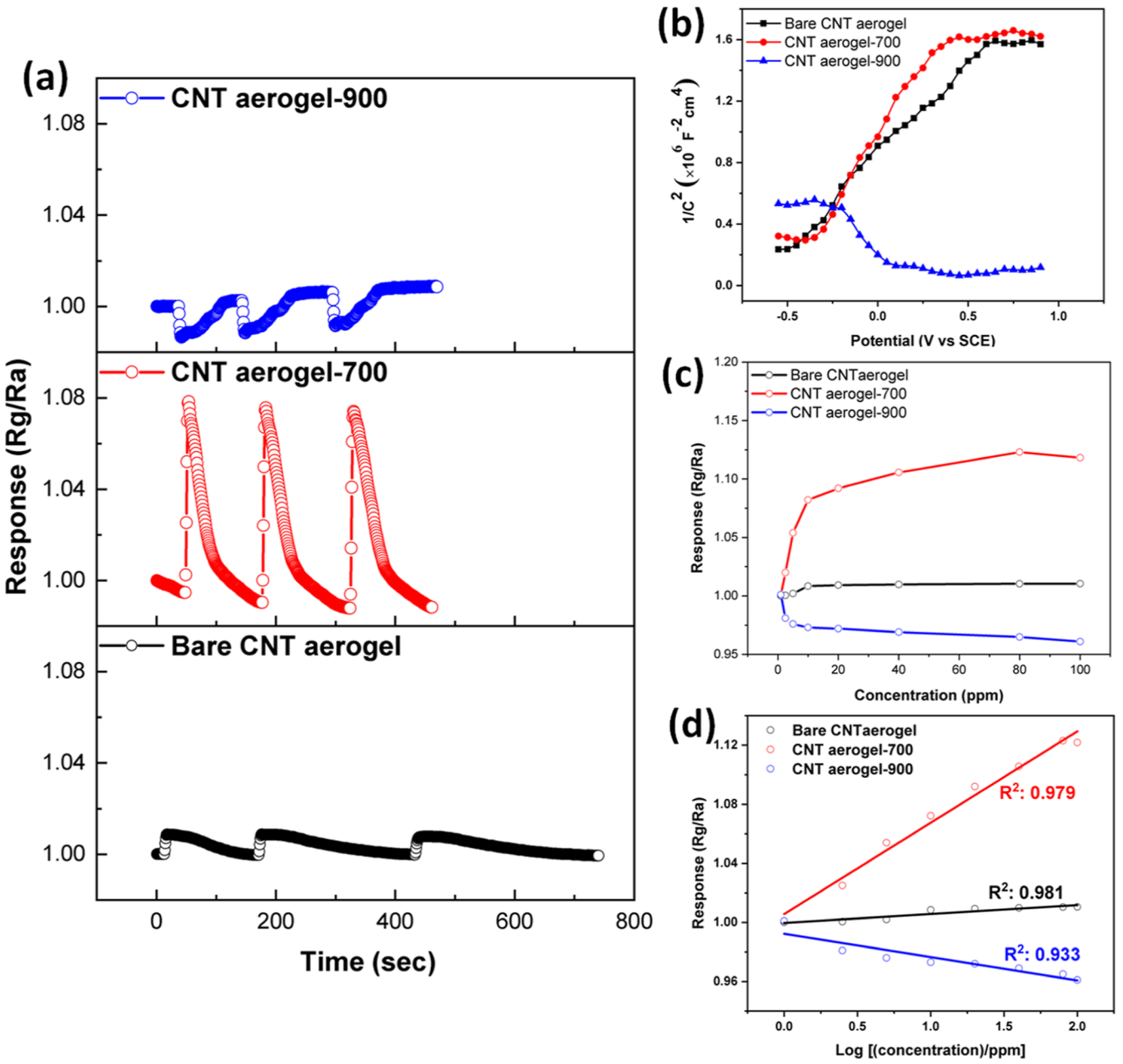

Figure 5. (a) Transient resistance response curve (repeating three cycle each) of bare and treated CNT aerogel sensors operating at room temperature (28 °C), RH: 45% for 10 ppm concentration of methanol. (b) M−S measurements plot carried out with a frequency of 1 kHz, (c) variation of the sensor response with methanol concentration (1−100 ppm), and corresponding (d) linear fitting.

decomposition of acetylene, consequently, the pore size decrease in this sample. However, the pore size in the CNT aerogel-900 sample increases in comparison to the CNT aerogel-700 sample may be because of lower decomposition kinetics of acetylene to carbon soot and conversion of amorphous carbon to ordered phase. The carbon soot along with the CNT network in CNT aerogel film is desired for improving gas adsorption for sensing purposes, as it improves the gas adsorption property of the film (Figure 2e).

To investigate the compatibility of synthesized bare and treated CNT aerogel films as nanoelectronic devices, the electronic transport properties of the films in two electrode configurations were measured (Supporting Information, Figure S1). It was observed that the air resistance of the bare CNT aerogel film increased after heat treatment and all samples showed Ohmic behavior with a stable current. The dense network of CNT in bare and treated CNT aerogel film facilitates in obtaining stable electronic conductivity. Therefore, the free-standing and flexible bare treated CNT aerogel films with excellent electronic conductivity can be suitably applied for gas sensing applications.

3.1. Methanol Gas Sensing. The bare CNT aerogel sensor showed a response in terms of an increase in resistance (R_g/R_a) as soon as methanol gas comes into contact with the sensor surface (Figure 5a; corresponding resistance response curve is shown in Supporting Information, Figure S4). The sensor response reaches a peak and recovers well to the baseline as soon as methanol gas is cut off. It is observed that the methanol sensing performance of the CNT aerogel-700 sensor significantly improved in comparison to the bare CNT

https://doi.org/10.1021/acsomega.2c07314
ACS Omega 2023, 8, 6708−6719

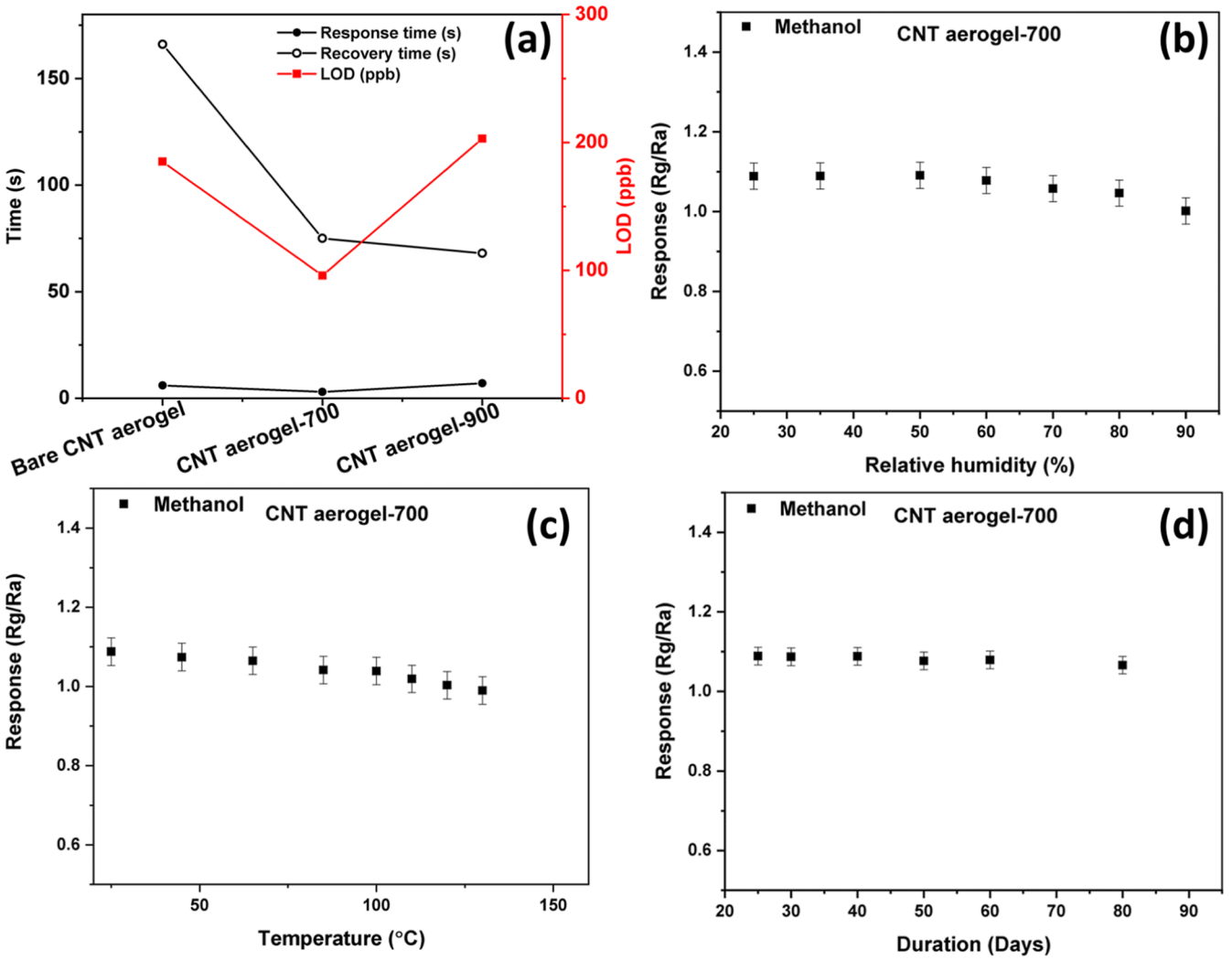

Figure 6. CNT aerogel-700 sensor (a) response/recovery time and LOD, (b) response under different RH conditions at room temperature (28 °C) for 10 ppm concentration of methanol, (c) different operating temperatures, and (d) stability of CNT aerogel-700 sensor operating at room temperature (28 °C) and RH: 45% for 10 ppm concentration of methanol.

aerogel sensor. However, the CNT aerogel-900 sensor showed lower but opposite sensing characteristics, that is, decrease in resistance as soon as methanol gas comes into contact with the sensor surface. Therefore, the CNT aerogel-900 sensor showed a switch in characteristic, and to explain this characteristic, sensor's semiconductor nature was analyzed by Mott−Schottky (M−S) measurements (Figure 5b). The positive slope of the M−S curve for bare and CNT aerogel-700 sensors confirmed their p-type semiconductor nature. However, negative slope in the M−S plot of the CNT aerogel-900 sensor confirmed its n-type semiconducting nature. Therefore, it is concluded that the semiconductor nature of the CNT aerogel-900 sensor switches to n-type from p-type. The switch in the semiconductor nature is the reason for the opposite response observed for the CNT aerogel-900 sensor. The transient resistance response curve (Figure 5a) shows the same type of sensing characteristics with a small deviation for repeated exposure to methanol which in turn reflects the reproducibility of the bare and treated CNT aerogel sensors.

Further response (R_g/R_a) of sensors were measured at room temperature (28 °C; RH: 45%) by varying the concentration of methanol gases from 1 to 100 ppm (Figure 5c). The CNT aerogel-700 sensor showed the highest sensitivity (0.12 Ω/ppm cm^{-2}), followed by the CNT aerogel-900 (0.011 Ω/ppm cm^{-2}) and bare CNT aerogel (0.004 Ω/ppm cm^{-2}) sensors. It is observed that the response was proportional to the logarithm of the methanol gas concentration (Figure 5d), indicating that our sensor is suitable for methanol gas quantification. The linear regression equation $R_g/R_a = \alpha + \beta \ln C$ (where α is intercepted, β is the slope, and C is the concentration of methanol gas) was fitted with a correlation coefficient. The obtained adjusted R^2 values >0.97, suggested that the linear regression fitting is appropriate for describing the detection ability of methanol, especially using the CNT aerogel-700 sensor. As observed from Figure 6a, the response time for the three sensors is comparable and in the range of 3−7 s; however, recovery time decreases for the CNT aerogel-700/900 sensor (~75/68 s) in comparison to the bare CNT aerogel sensor (176 s). The limit of detection (LOD) was estimated using "3σ/slope" formulae, as per the International Union of Pure and Applied Chemistry (IUPAC) guidelines.[29] The CNT aerogel-700 sensor showed the lowest LOD ~96 ppb. The humidity response curve (Figure 6b) showed that the CNT aerogel-700 sensor response does not change significantly in the RH of 25−60%. However, beyond humidity level of 60% the sensor was very sensitive to the humidity and the response

https://doi.org/10.1021/acsomega.2c07314
ACS Omega 2023, 8, 6708−6719

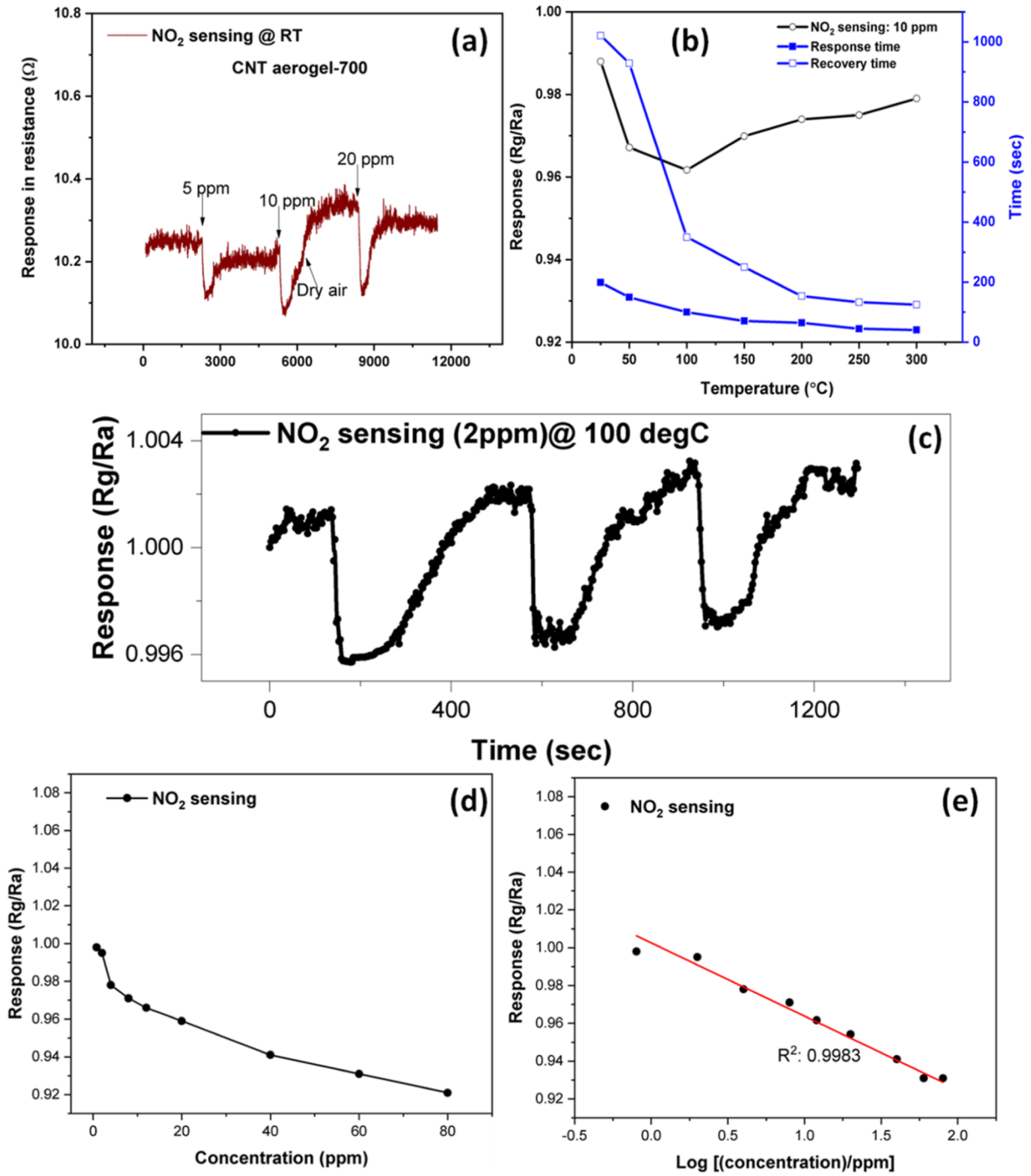

Figure 7. CNT aerogel-700 response curve for NO_2 sensing (a) operated at room temperature (28 °C), (b) varying operation temperature using 10 ppm of NO_2, (c) transient response curve for three cycles using 2 ppm of NO_2, (d) variation of the sensor response with NO_2 concentration (1−80 ppm), and corresponding (d) linear fitting to obtain LOD.

decreased with a further increase in humidity. It seems that the water molecules get absorbed on the sensor surface under higher humid conditions and it hinders methanol gas adsorption on the MWCNT surface present in the sensor, therefore decreasing the sensor response. The temperature variation response curve (Figure 6c; measured at a RH of 45%) showed that the sensor response decreases with an increase in sensor temperature, specifically sensor response drastically decreases after 75 °C. The observed decrease in response with the increase in temperature may occur due to the lower interaction of high volatile methanol gas on the higher temperature surface of the sensor. The stability of the CNT aerogel-700 sensor is also investigated to evaluate the probability in practical applications. As shown in Figure 6d, the CNT aerogel-700 sensor response to 10 ppm of methanol fluctuated less than 7% for 80 days, which reflects the acceptable long-term stability of the investigated sensor.

The sensitivity of the CNT aerogel-700 sensor toward the detection of the oxidizing nitrogen dioxide (NO_2) was further evaluated and shown in Figure 7a. The CNT aerogel-700 sensor showed a response in terms of a decrease in resistance as soon as oxidizing NO_2 gas comes into contact with the

https://doi.org/10.1021/acsomega.2c07314
ACS Omega 2023, 8, 6708−6719

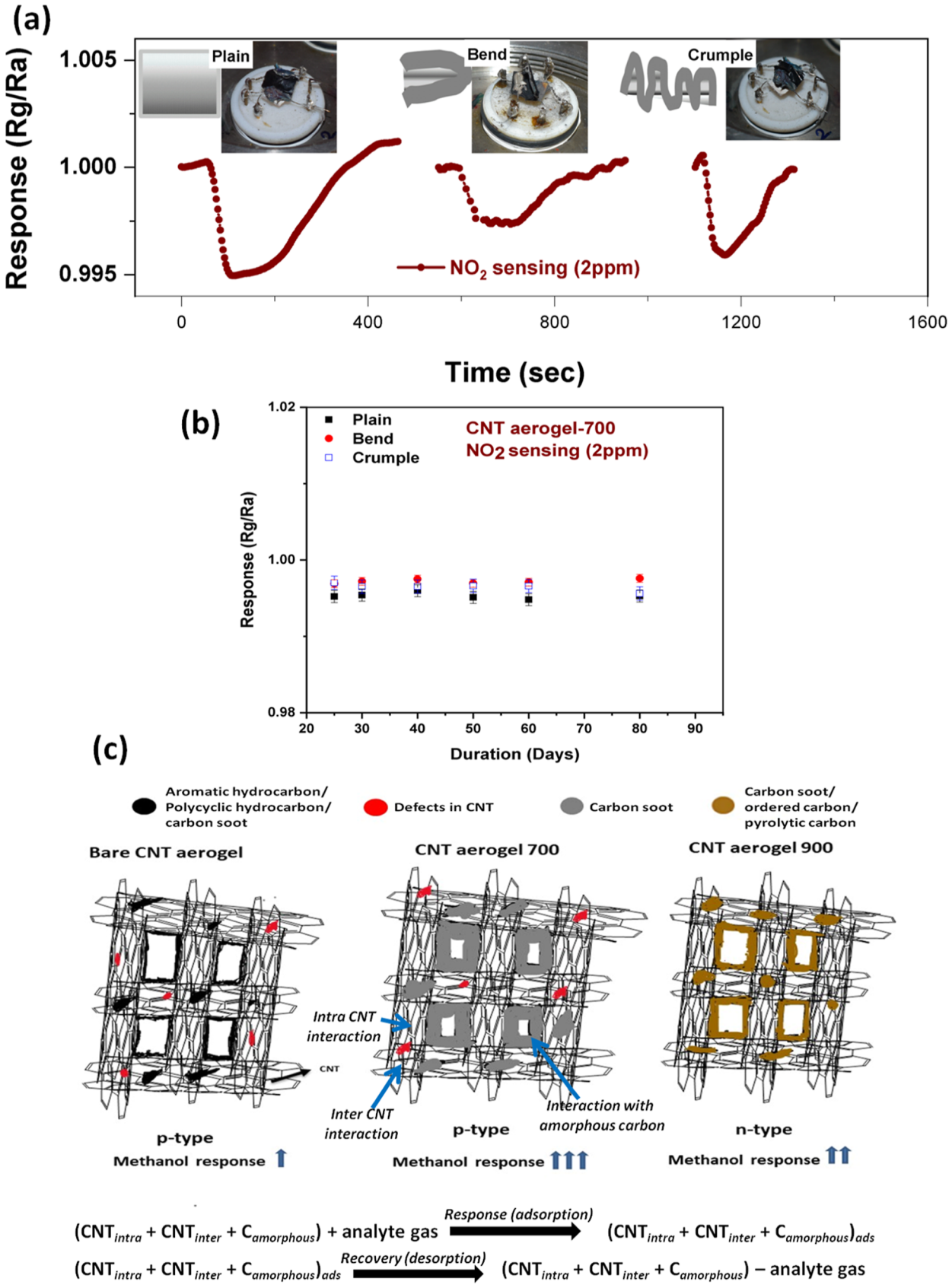

Figure 8. (a) Flexible sensing test of the CNT aerogel-700 film and (b) proposed sensing mechanism in bare and heat-treated CNT aerogel sensors.

sensor surface (p-type semiconductor). The sensor showed a very good response for 5, 10, and 20 ppm of NO_2 gas at room temperature with a response time of ~149 s (10 ppm NO_2) but the recovery was very slow (recovery time ~1520 s). To

https://doi.org/10.1021/acsomega.2c07314
ACS Omega 2023, 8, 6708−6719

improve the sensor response, the NO_2 sensing (10 ppm) experiment was carried out by varying the CNT aerogel-700 sensor temperature from 30 to 300 °C and shown in Figure 7b. It was observed that the sensor response increases upto 100 °C and decreases with a further increase in sensor temperature. It is concluded that the CNT aerogel-700 sensor showed the highest response with a moderately low response (~21 s)/ recovery time (~306 s) for 10 ppm NO_2 sensing at an operating temperature of 100 °C. The transient response curve (Figure 7c) shows the same type of sensing characteristics with a small deviation for repeated exposure to NO_2 gas which in turn reflects the reproducibility of the CNT aerogel-700 sensor.

The CNT aerogel-700 sensor response was further evaluated at an operating temperature of 100 °C by varying the NO_2 gas concentration (1−80 ppm) and shown in Figure 7d. The CNT aerogel-700 sensor responded well in the concentration range of 1−80 ppm and response increases with an increase in NO_2 gas concentration. It is observed that the response was proportional to the logarithm of the NO_2 gas concentration (Figure 7e), indicating that our sensor is suitable for NO_2 gas quantification. The fitted linear regression equation with R^2 values >0.99, suggested that the linear regression fitting is appropriate for describing the detection ability of the CNT aerogel-700 sensor. The estimated LOD of the CNT aerogel-700 sensor is 89 ppb, which is remarkable for the ultra-sensitive detection of NO_2 gas.

The flexibility of the CNT aerogel-700 film as a sensor was confirmed by evaluating its NO_2 sensing (2 ppm) performance in different physical conditions like plain, bend, and crumple (Figure 8a) at 100 °C operating temperature. The CNT aerogel-700 sensor showed a response in bend and crumple conditions for NO_2 gas. However, the intensity of response decreases with respect to the plain sensor. As shown in Figure 8b, the CNT aerogel-700 sensor showed consistent response to 2 ppm of NO_2 in different physical conditions for 80 days. A performance comparison between the fabricated-sensor and the reported CNT sensors is provided in Supporting Information, Table S1. It can be clearly seen that the response and response time of our CNT aerogel electrode are comparatively better than the other conventional bare/doped CNT-based electrodes. These results confirmed that the CNT aerogel-700 sensor can be used as a flexible and standalone sensor for long-term toxic NO_2 gas sensing.

The sensing mechanism of bare and treated CNT aerogel sensors is explained based on the interaction of analyte gases to the surface of the sensor (Figure 8c). The sensor response noticed in the presence of analyte gases can be attributed to two possible reasons: (i) surface interaction and diffusion of analyte molecules: which leads to response (ii) de-absorption: which leads to recovery. As concluded from Raman and TGA studies, the bare CNT aerogel film contains majorly large hydrocarbons, PAH, and a small quantity of carbon soot along with the CNT, whereas the CNT aerogel-700 sensor consists of majorly amorphous carbon in form of soot, and the CNT aerogel-900 sensor consists of majorly ordered phase carbon like pyrolytic carbon.[28] In the case of a bare CNT aerogel sensor, the response can be generated primarily due to the intra/inter CNT interaction of analyte gases. The CNT aerogel-700 showed a response due to the intra/inter CNT and amorphous carbon interaction with analyte gases and shown in Figure 8c. The CNT aerogel-700 sensor has a comparatively large amount of amorphous carbon soot and this amorphous carbon soot has better gas adsorption properties than aromatic hydrocarbon/PAHs. Therefore, the CNT aerogel-700 sensor showed a much better response to the analyte gases. In the case of the CNT aerogel-900 sensor, the amorphous carbon soot content decreases and thereby its response decreases in comparison to the CNT aerogel-700 sensor. Therefore, the sensitivity of the resistance-based CNT aerogel-700 sensor depends solely on the analyte gas diffusion, amorphous carbon soot content, and the number, and arrangement of CNT junctions in the sensor.[30−32] The selectivity of the CNT aerogel-700 sensor has been confirmed by sensing performance evaluation of different gases like methanol, ethanol, acetone, and NO_2 (Supporting Information, Figure S6). It is observed that methanol and NO_2 gases showed distinguished peak responses in comparison to other gases. The presence of comparatively smaller pores and a large number of gas adsorption sites due to the presence of amorphous carbon in the CNT aerogel-700 sensor enhanced the kinetics of selective diffusion of smaller molecules like methanol and NO_2 gases. This is the possible reason for the higher response of the fabricated sensors to NO_2 and methanol gases. As seen in Figure 5a (methanol sensing) and Figure 7c (NO_2 sensing), there was a small deviation in sensitivity in repeated three exposure cycles of the same concentration of analyte gases, which might occur due to incomplete desorption of the deeply adsorbed analyte gases in the sensor film before introducing the next cycle of analyte gases. Moreover, the CNT aerogel-700 sensor showed different response/recovery times and responses for different analyte gases, which might be due to the different chemical nature of analyte gases leading to the different molecular dipole interaction with CNT and amorphous carbon present in the sensor.

4. CONCLUSIONS

In the present work, we report the fabrication of a flexible and free-standing thin CNT aerogel film using a simple floating chemical vapor deposition process. The bare CNT aerogel samples synthesized using ethanol precursor contains ~20% amorphous carbon majorly in the form of large hydrocarbon/ polycyclic hydrocarbon. The CNT aerogel film was heat treated in a diluted acetylene atmosphere to enhance sensitivity and ease of transfer from one substrate to another. The CNT aerogel film heat treated at 700 °C showed a decrease in surface porosity and an increase in defects due to the conversion of large hydrocarbon/polycyclic hydrocarbon to carbon soot deposited along with the CNT network in the CNT aerogel film. Whereas in the case of a CNT aerogel film heat treated at 900 °C, the large hydrocarbon/polycyclic hydrocarbon converts to the more ordered phase of carbon like pyrolytic carbon. The CNT aerogel film treated at 700 °C, showed the highest response and sensitivity for methanol gas. However, film treated at 900 °C showed lower response with opposite sensing characteristic due to switching of the semiconductor nature of the CNT aerogel film to n-type from p-type. The CNT aerogel film treated at 700 °C has shown a very good response for toxic NO_2 gas, even in bending and crumple conditions. The developed electrical conducting, highly sensitive, and flexible chemiresistive CNT aerogel sensor paves the way for mass production with good repeatability and reliability for toxic gases such as methanol and NO_2 sensing.

https://doi.org/10.1021/acsomega.2c07314
ACS Omega 2023, 8, 6708−6719

■ ASSOCIATED CONTENT

Supporting Information

The Supporting Information is available free of charge at https://pubs.acs.org/doi/10.1021/acsomega.2c07314.

Electrical conductivity plot of CNT aerogel films, schematic and picture of the static/dynamic gas sensing unit, CNT aerogel sensors response curve in resistance, BET isotherm of CNT aerogel films, details on the SAXS study, transient resistance response curve of the CNT aerogel-700 sensor for different gases, and literature report on CNT-based VOC sensors (PDF)

Sticking test of CNT aerogel films (MOV)

■ AUTHOR INFORMATION

Corresponding Author

Jyoti Prakash − *Materials Group, Bhabha Atomic Research Centre, Mumbai 400085, India; Homi Bhabha National Institute, Mumbai 400094, India;* orcid.org/0000-0002-3011-6333; Phone: +91 2225593924; Email: jprakash@barc.gov.in

Authors

Pandugula Thirmaleshwar Rao − *Materials Group, Bhabha Atomic Research Centre, Mumbai 400085, India*

Rohan Rohilla − *Materials Group, Bhabha Atomic Research Centre, Mumbai 400085, India; Homi Bhabha National Institute, Mumbai 400094, India*

Divya Nechiyil − *Materials Group, Bhabha Atomic Research Centre, Mumbai 400085, India*

Manmeet Kaur − *Technical Physics Division, Bhabha Atomic Research Centre, Mumbai 400085, India; Homi Bhabha National Institute, Mumbai 400094, India;* orcid.org/0000-0002-0008-3630

Kailasa S. Ganapathi − *Technical Physics Division, Bhabha Atomic Research Centre, Mumbai 400085, India*

Anil Krishna Debnath − *Technical Physics Division, Bhabha Atomic Research Centre, Mumbai 400085, India; Homi Bhabha National Institute, Mumbai 400094, India*

Amit Kaushal − *Materials Group, Bhabha Atomic Research Centre, Mumbai 400085, India*

Jitendra Bahadur − *Solid State Physics Division, Bhabha Atomic Research Centre, Mumbai 400085, India;* orcid.org/0000-0002-2547-2907

Kinshuk Dasgupta − *Materials Group, Bhabha Atomic Research Centre, Mumbai 400085, India; Homi Bhabha National Institute, Mumbai 400094, India;* orcid.org/0000-0002-5742-7799

Complete contact information is available at: https://pubs.acs.org/10.1021/acsomega.2c07314

Notes

The authors declare no competing financial interest.

■ ACKNOWLEDGMENTS

The authors will like to acknowledge Dr. Purushottam Jha, BARC for helping with contact angle measurement.

■ REFERENCES

(1) Wongchoosuk, C.; Wisitsoraat, A.; Tuantranont, A.; Kerdcharoen, T. Portable Electronic Nose Based on Carbon Nanotube-SnO2 Gas Sensors and Its Application for Detection of Methanol Contamination in Whiskeys. *Sens. Actuators, B* **2010**, *147*, 392−399.

(2) Jambhulkar, S.; Xu, W.; Ravichandran, D.; Prakash, J.; Mada Kannan, A. N.; Song, K. Scalable Alignment and Selective Deposition of Nanoparticles for Multifunctional Sensor Applications. *Nano Lett.* **2020**, *20*, 3199−3206.

(3) Cho, S. Y.; Yu, H.; Choi, J.; Kang, H.; Park, S.; Jang, J. S.; Hong, H. J.; Kim, I. D.; Lee, S. K.; Jeong, H. S.; et al. Continuous Meter-Scale Synthesis of Weavable Tunicate Cellulose/Carbon Nanotube Fibers for High-Performance Wearable Sensors. *ACS Nano* **2019**, *13*, 9332−9341.

(4) Leghrib, R.; Felten, A.; Pireaux, J. J.; Llobet, E. Gas Sensors Based on Doped-CNT/SnO2 Composites for NO 2 Detection at Room Temperature. *Thin Solid Films* **2011**, *520*, 966−970.

(5) Duan, Y.; Pirolli, L.; Teplyakov, A. V. Investigation of the H2S Poisoning Process for Sensing Composite Material Based on Carbon Nanotubes and Metal Oxides. *Sens. Actuators, B* **2016**, *235*, 213−221.

(6) Badhulika, S.; Myung, N. V.; Mulchandani, A. Conducting Polymer Coated Single-Walled Carbon Nanotube Gas Sensors for the Detection of Volatile Organic Compounds. *Talanta* **2014**, *123*, 109−114.

(7) Mondal, R. K.; Dubey, K. A.; Kumar, J.; Jagannath; Bhardwaj, Y. K.; Melo, J. S.; Varshney, L. Carbon Nanotube Functionalization and Radiation Induced Enhancements in the Sensitivity of Standalone Chemiresistors for Sensing Volatile Organic Compounds. *ACS Appl. Nano Mater.* **2018**, *1*, 5470−5482.

(8) Norizan, M. N.; Moklis, M. H.; Ngah Demon, S. Z.; Halim, N. A.; Samsuri, A.; Mohamad, I. S.; Knight, V. F.; Abdullah, N. Carbon Nanotubes: Functionalisation and Their Application in Chemical Sensors. *RSC Adv.* **2020**, *10*, 43704−43732.

(9) Prakash, J.; Venugopalan, R.; Tripathi, B. M.; Ghosh, S. K.; Chakravartty, J. K.; Tyagi, A. K. Chemistry of One Dimensional Silicon Carbide Materials: Principle, Production, Application and Future Prospects. *Prog. Solid State Chem.* **2015**, *43*, 98−122.

(10) Pandhi, T.; Chandnani, A.; Subbaraman, H.; Estrada, D. A Review of Inkjet Printed Graphene and Carbon Nanotubes Based Gas Sensors. *Sensors* **2020**, *20*, 5642.

(11) Kossyvaki, D.; Barbetta, A.; Contardi, M.; Bustreo, M.; Dziza, K.; Lauciello, S.; Athanassiou, A.; Fragouli, D. Highly Porous Curcumin-Loaded Polymer Mats for Rapid Detection of Volatile Amines. *ACS Appl. Polym. Mater.* **2022**, *4*, 4464−4475.

(12) Zhang, M.; Inoue, S.; Matsumura, Y. Light and Flexible Gas Sensors Made of Free-Standing Carbon Nanotube Paper. *Chem. Phys. Lett.* **2020**, *747*, 137367.

(13) Xue, L.; Wang, W.; Guo, Y.; Liu, G.; Wan, P. Flexible Polyaniline/Carbon Nanotube Nanocomposite Film-Based Electronic Gas Sensors. *Sens. Actuators, B* **2017**, *244*, 47−53.

(14) Agarwal, P. B.; Alam, B.; Sharma, D. S.; Sharma, S.; Mandal, S.; Agarwal, A. Flexible NO2 Gas Sensor Based on Single-Walled Carbon Nanotubes on Polytetrafluoroethylene Substrates. *Flexible Printed Electron.* **2018**, *3*, 035001.

(15) McConnell, C.; Kanakaraj, S. N.; Dugre, J.; Malik, R.; Zhang, G.; Haase, M. R.; Hsieh, Y. Y.; Fang, Y.; Mast, D.; Shanov, V. Hydrogen Sensors Based on Flexible Carbon Nanotube-Palladium Composite Sheets Integrated with Ripstop Fabric. *ACS Omega* **2020**, *5*, 487−497.

(16) Geng, Y.; Ren, Y.; Wang, X.; Li, J.; Portilla, L.; Fang, Y.; Zhao, J. Highly Sensitive and Selective H2S Sensors with Ultra-Low Power Consumption Based on Flexible Printed Carbon-Nanotube-Thin-Film-Transistors. *Sens. Actuators, B* **2022**, *360*, 131633.

(17) Chang, S.; Yang, M.; Pang, R.; Ye, L.; Wang, X.; Cao, A.; Shang, Y. Intrinsically Flexible CNT-TiO2-Interlaced Film for NO Sensing at Room Temperature. *Appl. Surf. Sci.* **2022**, *579*, 152172.

(18) Seo, S. G.; Baek, J. I.; Mishra, D.; Jo, H.; Kwon, H. I.; Jin, S. H. One-Pot Hydrothermal Growth of Indium Oxide-CNT Heterostructure via Single Walled Carbon Nanotube Scaffolds and Their Application toward Flexible NO2 Gas Sensors. *J. Alloys Compd.* **2022**, *922*, 166169.

(19) Kröning, K.; Krause, B.; Pötschke, P.; Fiedler, B. Nanocomposites with P-and n-Type Conductivity Controlled by Type and Content of Nanotubes in Thermosets for Thermoelectric Applications. *Nanomaterials* **2020**, *10*, 1144.
(20) Yadav, M. D.; Dasgupta, K. Kinetics of Carbon Nanotube Aerogel Synthesis Using Floating Catalyst Chemical Vapor Deposition. *Ind. Eng. Chem. Res.* **2021**, *60*, 2187−2196.
(21) Ramgir, N. S.; Ghosh, M.; Veerender, P.; Datta, N.; Kaur, M.; Aswal, D. K.; Gupta, S. K. Growth and Gas Sensing Characteristics of P- and n-Type ZnO Nanostructures. *Sens. Actuators, B* **2011**, *156*, 875−880.
(22) Esarte, C.; Peg, M.; Ruiz, M. P.; Millera, Á.; Bilbao, R.; Alzueta, M. U. Pyrolysis of Ethanol: Gas and Soot Products Formed. *Ind. Eng. Chem. Res.* **2011**, *50*, 4412−4419.
(23) Minakov, A. V.; Simunin, M. M.; Ryzhkov, I. I. Modelling of Ethanol Pyrolysis in a Commercial CVD Reactor for Growing Carbon Layers on Alumina Substrates. *Int. J. Heat Mass Transfer* **2019**, *145*, 118764.
(24) Richter, H.; Howard, J. B. Formation of Polycyclic Aromatic Hydrocarbons and Their Growth to Soot—a Review of Chemical Reaction Pathways. *Prog. Energy Combust. Sci.* **2000**, *26*, 565−608.
(25) Rokstad, O. A.; Lindvaag, O. A.; Holmen, A. Acetylene Pyrolysis in Tubular Reactor. *Int. J. Chem. Kinet.* **2014**, *46*, 104−115.
(26) Sánchez, N. E.; Callejas, A.; Millera, Á.; Bilbao, R.; Alzueta, M. U. Polycyclic Aromatic Hydrocarbon (PAH) and Soot Formation in the Pyrolysis of Acetylene and Ethylene: Effect of the Reaction Temperature. *Energy Fuels* **2012**, *26*, 4823−4829.
(27) Saggese, C.; Sánchez, N. E.; Frassoldati, A.; Cuoci, A.; Faravelli, T.; Alzueta, M. U.; Ranzi, E. Kinetic Modeling Study of Polycyclic Aromatic Hydrocarbons and Soot Formation in Acetylene Pyrolysis. *Energy Fuels* **2014**, *28*, 1489−1501.
(28) Zhao, S.; Shi, J.; Wei, X.; Yan, X.; Guo, Q.; Liu, L. Preparation of Pyrolytic Carbon Coating from Acetylene by Cold Wall Chemical Vapour Deposition Process. *Asian J. Chem.* **2013**, *25*, 871−873.
(29) Long, G. L.; Winefordner, J. D. Limit of Detection A Closer Look at the IUPAC Definition. *Anal. Chem.* **1983**, *55*, 712A.
(30) Siwal, S. S.; Saini, A. K.; Rarotra, S.; Zhang, Q.; Thakur, V. K. Recent Advancements in Transparent Carbon Nanotube Films: Chemistry and Imminent Challenges. *J. Nanostruct. Chem.* **2021**, *11*, 93−130.
(31) Leghrib, R.; Dufour, T.; Demoisson, F.; Claessens, N.; Reniers, F.; Llobet, E. Gas Sensing Properties of Multiwall Carbon Nanotubes Decorated with Rhodium Nanoparticles. *Sens. Actuators, B* **2011**, *160*, 974−980.
(32) Li, C.; Yang, S.; Guo, Y.; Huang, H.; Chen, H.; Zuo, X.; Fan, Z.; Liang, H.; Pan, L. Flexible, Multi-Functional Sensor Based on All-Carbon Sensing Medium with Low Coupling for Ultrahigh-Performance Strain, Temperature and Humidity Sensing. *Chem. Eng. J.* **2021**, *426*, 130364.

https://doi.org/10.1021/acsomega.2c07314
ACS Omega 2023, 8, 6708−6719